LEVEL II

(12) 2-

JOINT INSTITUTE FOR LABORATORY ASTROPHYSICS

UNIVERSITY OF COLORADO
BOULDER, COLORADO 80309

UNIVERSITY OF COLORADO

NATIONAL BUREAU OF STANDARDS

SEMIANNUAL REPORT

RESEARCH IN LASER PROCESSES

Research Sponsored by
Advanced Research Projects Agency
and
Office of Naval Research

ARPA Order No. 2683, Amendment 4
Program Code No. 7E20
Contractor: University of Colorado
Effective Date of Contract: July 1, 1975
Contract Expiration Date: Sep. 30, 1977
Amount of Contract $310,000
Period Covered: February 1, 1977 to July 31, 1977

Contract No. N00014-76-C0123
Principal Investigators:
A. V. Phelps
Telephone: (303) 492-7850
A. C. Gallagher
Telephone: (303) 492-7841
Scientific Officer: Director, Physics Program, ONR
Short Title of Work: Laser Processes

April 21, 1978

The views and conclusions contained in this document are those of the authors and should not be interpreted as necessarily representing the official policies, either expressed or implied, of the Defense Advanced Research Projects Agency or the U.S. Government.

Cable Address: JILA

Telephone Number: 492-7789

DISCLAIMER NOTICE

THIS DOCUMENT IS BEST QUALITY PRACTICABLE. THE COPY FURNISHED TO DDC CONTAINED A SIGNIFICANT NUMBER OF PAGES WHICH DO NOT REPRODUCE LEGIBLY.

Unclassified

SECURITY CLASSIFICATION OF THIS PAGE (When Data Entered)

REPORT DOCUMENTATION PAGE	READ INSTRUCTIONS BEFORE COMPLETING FORM
1. REPORT NUMBER: None	2. GOVT ACCESSION NO. / 3. RECIPIENT'S CATALOG NUMBER
4. TITLE (and Subtitle): ~~Semiannual Report~~ (6) Research in Laser Processes.	5. TYPE OF REPORT & PERIOD COVERED: 1 Feb. 1977 to 31 July 1977
	6. PERFORMING ORG. REPORT NUMBER
7. AUTHOR(s): (10) A. V. Phelps ~~and~~ A. C. Gallagher	8. CONTRACT OR GRANT NUMBER(s): (15) N0014-76-C-0123; ARPA Order-2683
9. PERFORMING ORGANIZATION NAME AND ADDRESS: University of Colorado, Joint Institute for Laboratory Astrophysics, Boulder, CO 80309	10. PROGRAM ELEMENT, PROJECT, TASK AREA & WORK UNIT NUMBERS: NR 012-512/10-6-76, Code 421; ARPA Ord No. 2683, Amd. 4, Prog. Cd. 7E20
11. CONTROLLING OFFICE NAME AND ADDRESS: Office of Naval Research, Department of the Navy, 800 North Quincy St., Arlington, VA 22217	(11) 12. REPORT DATE: 21 April 1978; 13. NUMBER OF PAGES: 24
14. MONITORING AGENCY NAME & ADDRESS (if different from Controlling Office): (12) 26 p.	15. SECURITY CLASS. (of this report): Unclassified; 15a. DECLASSIFICATION/DOWNGRADING SCHEDULE

16. DISTRIBUTION STATEMENT (of this Report)

This document has been approved for public release and sale; its distribution is unlimited.

17. DISTRIBUTION STATEMENT (of the abstract entered in Block 20, if different from Report)

(9) Semi-annual rept. 1 Feb-31 Jul 77,

18. SUPPLEMENTARY NOTES

19. KEY WORDS (Continue on reverse side if necessary and identify by block number)

Laser, processes, sodium vapor, rare gas, electrical discharge, high pressure, molecules, metastables.

20. ABSTRACT (Continue on reverse side if necessary and identify by block number)

Measurements have been made of the electrical and optical properties of electrical discharges in Na-Xe mixtures at high pressures. Although the discharges show desirable features such as a positive volt-ampere characteristics, the excited state densities are too low for useful gain. Since this does not appear to be the case in Tl-Xe, experiments and modeling directed toward an explanation were initiated. Scaling laws for the cathode fall region of discharges in helium have been used to extend low pressure .....

→ next page

DD FORM 1 JAN 73 1473 EDITION OF 1 NOV 65 IS OBSOLETE

Unclassified

SECURITY CLASSIFICATION OF THIS PAGE (When Data Entered)

192 900

A sub u 3 Sigma (+) sub u

experimental results to high pressures. Measurements are being made of electron excitation rate coefficients for the $A^3\Sigma_u^+$ state of N_2 in the range of mean energies of laser interest. Predictions have been made of large decreases in optical pumping efficiency at the center of the resonance lines of metal vapors and experiments are underway to test the theory.

SEMIANNUAL REPORT

This Semiannual Report contains descriptions of work carried out under ONR Contract No. N00014-76-0123 and ARPA Order No. 2683-Amd. 4. It covers the period from 1 February 1977 to 31 July 1977. Section I is the Semiannual Report Summary while Sections II-V are more detailed descriptions of work carried out under the four projects supported by this contract.

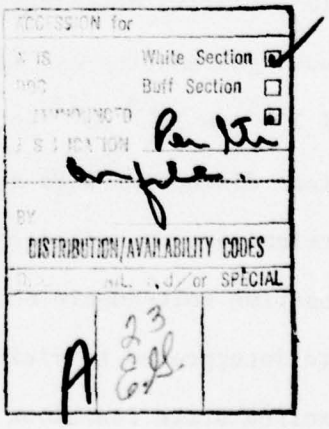

I. SEMIANNUAL REPORT SUMMARY

The four projects being carried out in the area of Laser Processes under this contract are summarized below. More detailed discussions are given in Sections II through V of this report.

(1) Metal Vapor-Rare Gas Discharges.

Metal vapor-rare gas molecules are attractive prospects as the active media for high efficiency, high power lasers operating at near visible wavelengths.[1,2] Our measurements of the optical properties of the alkali metal atom-rare gas molecules have been discussed in earlier reports in this series. Analyses of these data led us to the conclusion that electric discharges offered the possibility of efficient excitation of the alkali metal-rare gas excimers. Accordingly we have been engaged in an experimental and analytical evaluation of the potential for laser applications of electric discharge excitation of one of these systems, i.e., the Na-Xe system. This report contains a summary of the experimental results to date.

The experimental measurements of the optical and electrical characteristics electric discharges in Na-Xe were made under conditions as close as possible to those appropriate for laser applications. Thus, the high power (10-100 MW/ℓ) discharges were operated in a pulsed mode (~4 μsec) so as to avoid gas heating and at Na densities of 10^{15} to 10^{16} cm^{-3} and Xe densities of 10^{19} to 10^{20} cm^{-3} so as to maximize excimer formation. Stable quasi-steady-state discharges were obtained in a small volume cell without the use of preionizers or sustainers. This stability is attributed to the observed positive volt-ampere characteristics of the discharge. Measured spectra are interpreted to yield excited atom and excimer densities. The measured excited state fractions for the $Na(3^2P)$ atoms and for the $NaXe(A^2\Pi)$ excimer state are disappointingly low. These and other excited state densities are

close to those expected for an electron-excited state temperature of about 0.35 eV instead of about 0.5 eV as required for efficient excimer laser operation.

The modeling of the NaXe discharge has shown[3] that the electron impact excitation and ionization of highly excited states is much more important than previously thought. The reworking and generation of the required electron impact cross sections and rate equations continued throughout this report period.

(2) Stability of Discharges in Weakly Ionized Gases.

The problem being modeled is the growth and steady-state characteristics of the cathode fall region of a glow discharge such as used in high power discharges or discharge enhanced lasers. This region is particularly important in high pressure, high current density lasers because of the large amount of power dissipated in a small volume and the resultant potential for the growth of discharge nonuniformities, i.e., arcing. During the portion of this report period for which this project was active, it was found that scaling laws used in our earlier modeling at relatively low current densities could be used to correlate a wide range of published steady-state data.

(3) Electron Excitation of Molecular Metastables.

The technical problem addressed in this project is the prediction of rate coefficients for the excitation of the upper laser levels under discharge conditions. Such predictions are extremely valuable in the initial evaluation and optimization of discharge excited lasers. The present phase of this project is concerned with the measurement of excitation rate coefficients for the $A^3\Sigma_u^+$ state of the N_2 molecule. This metastable state has been proposed as

an efficient "transformer" of the discharge power into the energy of various upper laser levels, e.g., NO and Hg. Our preliminary results suggest that previous calculations of excitation rate coefficients for this state are much too high.

(4) Scattering and Transport of Resonance Excitation in Gases.

These experiments are intended to test our ability to predict the role of nonradiative transport of resonance excitation when metal vapors are optically pumped by lasers at wavelengths near the center of the resonance lines. Thus our recent calculations of this effect using a previously developed model predict that the efficiency of optical pumping of the resonance levels of Na decreases by an order of magnitude at line center for Na densities of about 3×10^{15} atom/cm^3. We have obtained some of the required experimental data but have not made quantitative comparisons with theory.

II. METAL VAPOR-RARE GAS DISCHARGES.

Drs. H. Rothwell, R. Shuker, A. Gallagher and Mr. D. Leep.

The immediate objective of this project is to determine whether electrical discharges in mixtures of Na vapor and high pressure Xe are good candidates for high power, high efficiency visible lasers. We have carried out this evaluation by measuring the electrical characteristics and emitted radiation from pulsed discharges in Na-Xe mixtures at [Na] = 10^{15}-10^{16} cm^{-3} and [Xe] = 3-6$\times10^{19}$ cm^{-3} and current densities from 10 to 250 A/cm^2.

A. Apparatus.

A sketch of the gas cell and discharge region is shown in Fig. 1. For details see Ref. 4. Temperatures ranging from 350-500°C are used to maintain Na in the desired saturated vapor density. Since Na vapor reacts with pyrex and quartz, a sapphire sleeve is used to help confine the

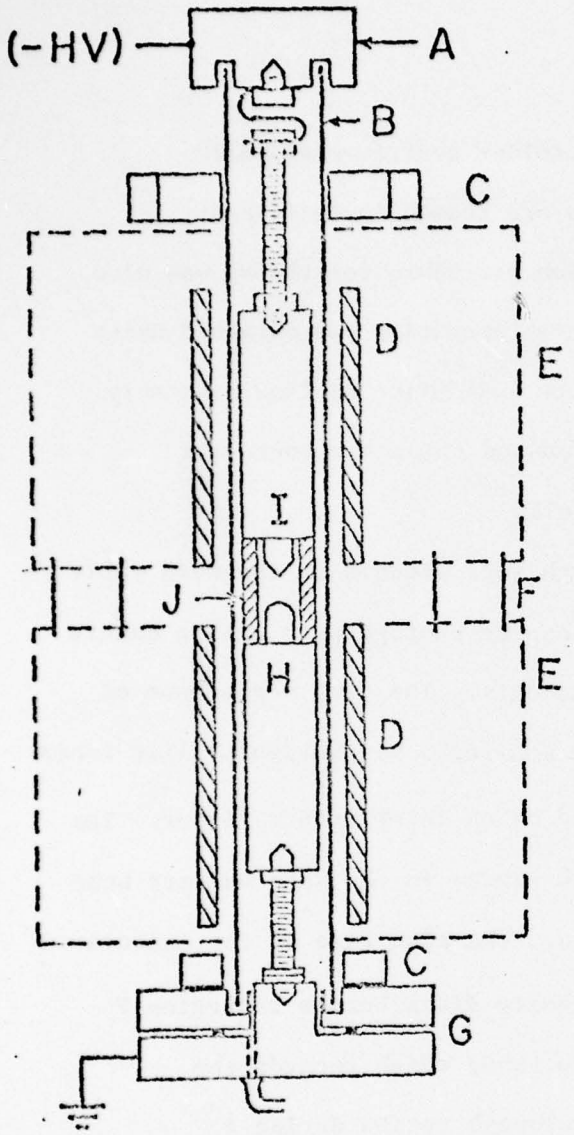

a

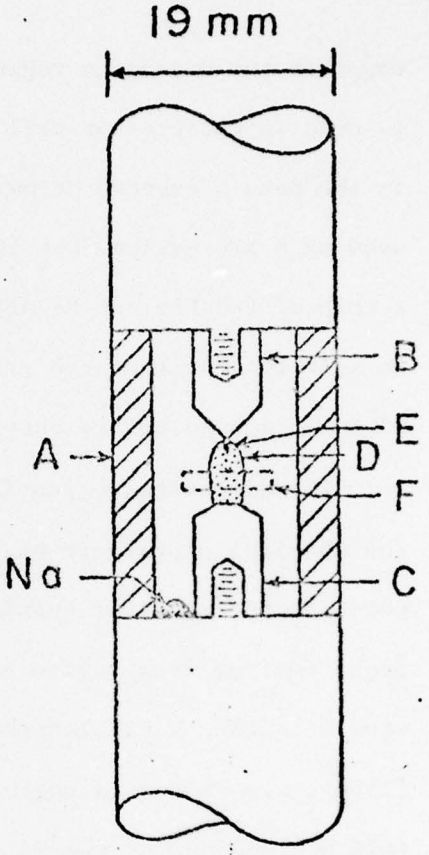

b

Fig. 1a) Discharge cell: A, stainless cap; B, quartz jacket, indium soldered to the top cap and bottom flange; C, water cooling; D, heater coils; E. firebrick enclosure; F, quartz windows; G, bottom flange and anode base with indium gasket seal; H, anode support (kovar); I. cathode support (kovar); J, sapphire tube; K, pump out and gas inlet.

b) Cross section of discharge region, drawn to scale for 5.3 mm gap. A, sapphire tube; B, cathode (molybdenum); C, anode (molybdenum); D, discharge positive column; E, cathode bright spot; F, viewed region for diagnostics of positive column.

vapor to the discharge region. An indium solder quartz-metal seal is used in the present cell and impurities are deemed insignificant in the data presented below. A distillation procedure for the Na was also used as a precaution, but identical discharge operation was obtained using a chip of freshly cut Na placed on the anode just prior to final assembly. In addition the research grade xenon was passed through a baked-out titanium sponge before entering the gas cell.

The discharge region is viewed through four windows in the oven wall. The physical appearance of the discharge can be photographed with a camera which is not used for quantitative measurements. The time dependence of light emitted from region F in Fig. 1b is monitored by photomultiplier tubes, each detecting a wavelength region defined by an interference filter. The filters are chosen to include a wavelength region in the NaXe excimer band (670 nm) and one at the Na resonance lines. The rise time of the associated electronics is 20 nsec. The spatial intensity distribution in region F in Fig. 1b is measured with an SIT vidicon tube, which records the total light emitted in the 630-640 nm wavelength region during a discharge pulse. The discharge spectrum is measured with a scanning 0.5-m spectrometer with ~3 Å resolution. The associated photomultiplier output is sampled in a specific time interval, typically centered at 2 μsec after onset of the discharge. Repetitive discharges are necessary for accumulation of a spectrum; the discharge repetition rate is limited to 10 Hz to avoid possible gas heating. The spectral sensitivity of the spectrometer and the photomultiplier sensitivities, as filtered, are measured using a diffuse reflector, illuminated by a calibrated

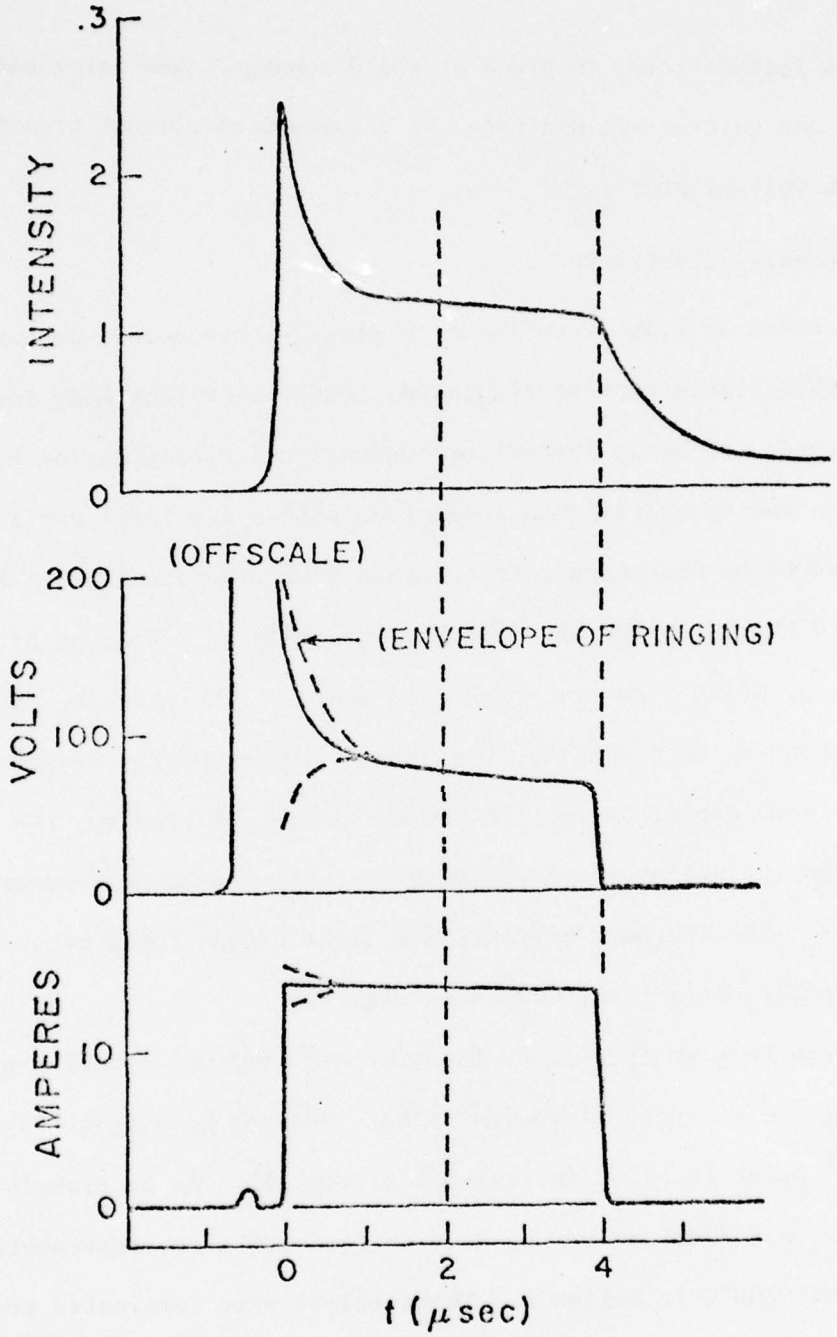

Fig. 2. Time dependences for a 4 μsec discharge. Light intensity from zone F in Fig. 1b at 562 nm (through an 0.5 nm half-width filter), total interelectrode voltage, and total discharge current are shown for [Na] = 6.3×10^{15} cm^{-3} and [Xe] = 4.4×10^{19} cm^{-3}.

tungsten iodiode lamp, in place of the discharge. The inter-electrode current and voltage are monitored by a commerical current transformer and high voltage probe.

B. Discharge Stability.

In order to allow comparison to steady-state models we have maintained the discharge in a current-regulated, constant-current mode for several microseconds following initial preionization. Preionization by a uv flashlamp and by multiphoton ionization with a dye laser was investigated but found to be unnecessary to maintain discharge stability. For the data presented the discharge was initiated by applying a voltage of ~4 kV across 0.5 cm gap, using a current-regulated pentode tube circuit. After 0.2-1 μsec, depending on densities, the current increased rapidly and discharged the electrode capacitances. Following ~1 μsec of ringing, the voltage settled in the neighborhood of 100 V with the discharge current regulated at 1-20 A. The current, voltage, and light output for a representative set of conditions are reproduced in Fig. 2.

As can be seen in Fig. 2, the discharge voltage slowly sagged during the (constant current) discharge pulse. The gas heating during this 4 μsec, 130 A/cm^2 pulse is ~70°C in region F of Fig. 1b. As an example of a longer discharge, a 7 A/cm^2 pulse was held on for ~100 μsec, representing a gas heating of ~200°C in region A. These pulses were terminated to protect the current regulating tetrode, so these values represent lower limits to the feasible energy deposition.

Initially, molybdenum button electrodes were used. Using only Xe vapor at 10^{19} - 10^{20} cm^{-3} density, a single filamentary arc would discharge between the electrodes, as is normally observed in pure noble-gases. But

at [Na] > 10^{14} cm^{-3}, the discharge homogeneously filled the volume between electrodes at a current I $\lesssim$ 0.5 A. At I $\gtrsim$ 1 A, the discharge would spread out from bright cathode spots, with the number of spots increasing with I. With the onset of cathode spots, the cathode fall voltage dropped from ~150 V to ~20 V. In order to control the positions and number of cathode spots, a conical molybdenum cathode of 90° full angle and buffed to a rounded point was then used. This cathode, combined with a 5 mm diameter flat anode was used for the results reported here. The electrode gap was normally 5.3 mm, except for a respacing to 10.0 mm to establish the fraction of the total voltage attributable to the cathode fall. At all [Na], [Xe], and currents (1-20 A) studied the discharge spread out from a small, bright spot at this cathode point into a homogeneous volume discharge, as indicated in Fig. 1b. The width of the discharge in the glow region (region F in Fig. 1b) was measured and found to increase with increasing I and decreasing N, with the anode size clearly limiting the discharge area in some cases. The size of the bright cathode spot and the widths of the glow discharge region were essentially constant during the several microseconds of discharge.

C. Results.

The emission spectrum is shown in Fig. 3 for two discharge conditions. The contribution of the NaXe A-X band,[5] the 4SΣ-XΣ band,[6] and the Na_2 A-X band[7] are identified in the figure along with lines from higher lying Na levels. The top spectrum is from the I < 0.5 A, homogeneous glow mode (current density ~7 A/cm^2). With the exception of a few Xe I lines beyond 800 nm and a trace amount of potassium, all emission from this discharge is attributed to excited Na. In the lower half of Fig. 3 spectra from two

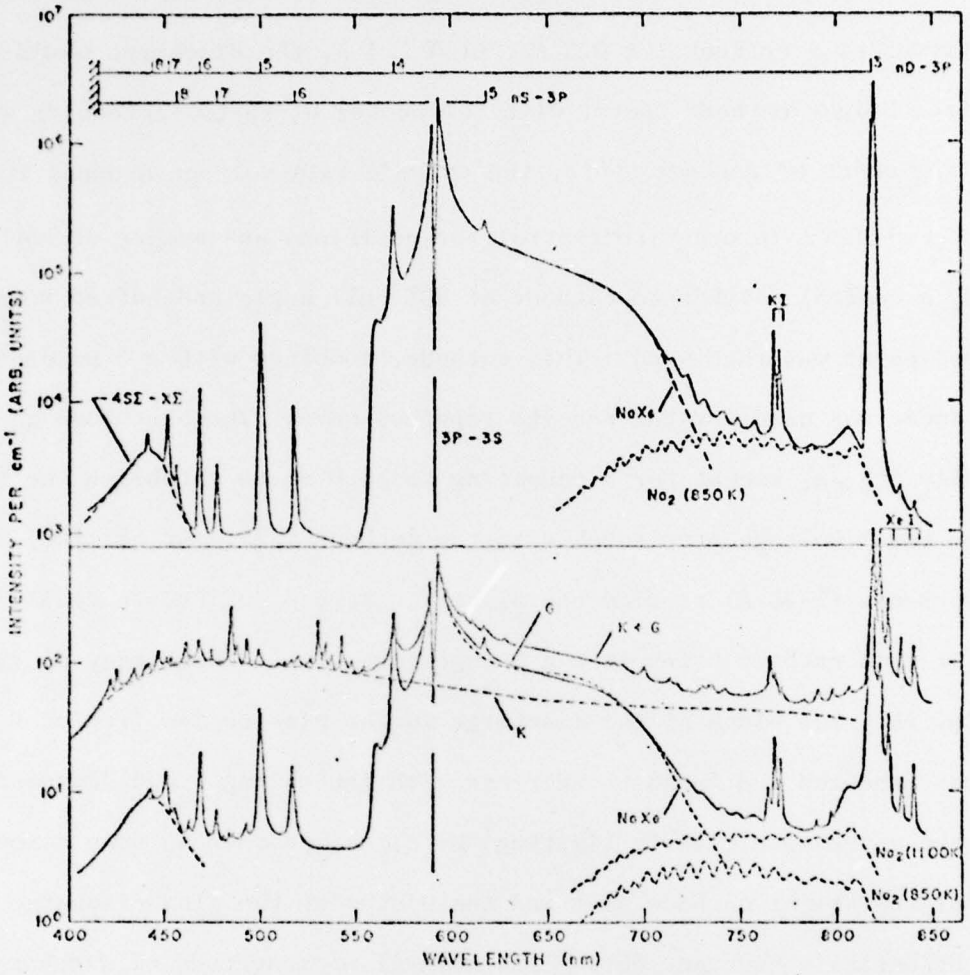

Fig. 3. Discharge intensity per unit frequency interval for two discharge conditions. Top spectrum: [Na] = 6.8×10^{15}; [Xe] = $2.8 \times 10^{19}/cm^3$; current density = 7 A/cm^2; inter-electrode voltage = 100 V. Bottom spectrum: K+G, from an 8 mm wide, 2 mm high zone that includes the cathode bright spot; G, from region F in Fig. 1b, in the positive column; K, difference between K+G and G spectrum, attributed to cathode bright spot. [Na] = $6.3 \times 10^{15}/cm^3$; [Xe] = $4.4 \times 10^{19}/cm^3$, current density = 130 A/cm^2, E/N = 3×10^{-18} $V\text{-}cm^2$. The $Na_2(A\text{-}X)$ bands, from a thermalized A-state, at the indicated temperatures, are from Ref. 7.

different spatial regions are compared. The solid line curves, G, is representative of a high current density (~130 A/cm^2) discharge spectrum for light emitted from the positive column region, region F in Fig. 1b. The curve labeled K + G is typical of light originating from a ~2 mm high, 4 mm wide zone that includes the cathode. Since light from outside the cathode spot is included in this, we have estimated the spectrum of the cathode spot by subtracting the spectrum of zone A, normalized to remove the Na lines in the K + G spectrum. This yields the line labeled K, which is assumed to characterize the cathode spot. This spectrum looks like a thermal continuum, and is similar to a high-pressure Xe flashlamp spectrum.

The dotted line labeled NaXe is the shape of the A-X band, as measured in Ref. 7 and adjusted to our operating temperature. The minor difference in the shape of the dotted curve could be due to an elevated vibrational temperature of the $NaXe^*$ A state. This could be due to electron collisions with $NaXe^*$ plus gas heating.

The regular intensity undulations in the 720-780 nm region in Fig. 3 are attributed to the Na_2 A-X band; as they match the expected positions of the A-X band peaks.[7] The emission spectrum from the Na_2 A-state with an 850 K thermal population distribution is shown in the top and bottom of Fig. 3, with an intensity sufficient to explain the observed intensity undulations in each case. In order to explain the total intensity in the 720-800 nm region for the 130 A/cm^2 case we then need to postulate an additional broad continuum, with intensity ~4 in units of Fig. 3; this appears consistent with the observed intensity in the 470-550 nm region.

However, the 720-800 nm intensity could also be attributed entirely to Na_2 A-X band from a thermal A-state population distribution at ~1100 K, as shown in the bottom of Fig. 3. Such an elevated temperature distribution could easily result from A-state collisional destruction before complete vibrational relaxation. The broad feature observed at 810 nm in both spectra may also be the Na_2, A-X band satellite,[7] but as can be inferred from the two Na_2 bands shown in Fig. 3 it is necessary to invoke a nonthermal A-state population distribution to explain both the satellite intensity and the magnitude of the intensity undulations in either spectrum. The actual Na_2 A-X band intensity thus remains somewhat uncertain, and one cannot tell if Na_2 A-state atoms are being depleted relative to NaXe A-state atoms at the higher current densities. Such depletion of Na_2 X and A-state molecules is expected to occur at high current densities, due to electron collisional dissociation of the X and A states.

Absolute intensity measurements of the NaXe A-X band, from region F in Fig. 1b, are reduced to a Na 3P density [Na(3P)] using the normalized emission data of Ref. 5 and the measured effective area. From this density, calculated transition probabilities,[8] and the discharge cross sectional area we can establish that, except for the 4S-3P and 3D-3P transitions, the nS-3P and nD-3P lines in Fig. 3 are optically thin. The total intensity from these line shapes thus equals $[Na(nS)]\Gamma_{nS-3P}$ and $[Na(nD)]\Gamma_{nD-3P}$, where Γ is the spontaneous emission rate. The resulting axial densities of various excited Na states, divided by their statistical weights, are plotted in Fig. 4 for two current densities. A lower limit to the residual (un-ionized) [Na(3S)] in the discharge can be obtained by subtracting the electron density n_e,

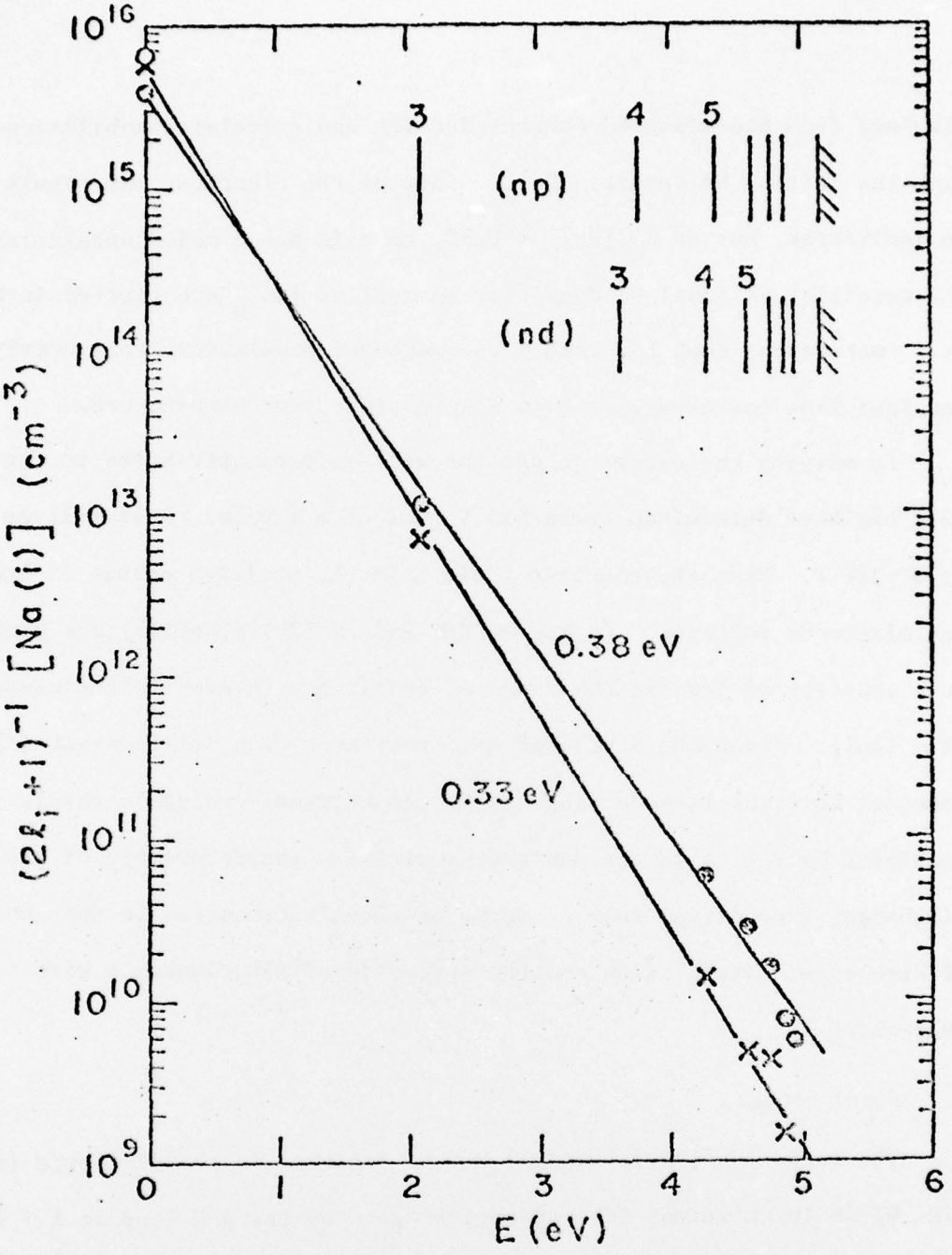

Fig. 4. Ratio of excited state population to statistical weight as a function of energy above the ground state, for [Xe] = 4.5×10^{19} cm^{-3}, an initial [Na] = 6.3×10^{15} cm^{-3} (o), and current density ≈130 A/cm^2 (•); 13 A/cm^2 (×). The density of [Na(3S)] during the discharge is indicated as (•) or (×); the 3S, 3P and nD, n = 4-8, state populations are given. The straight lines correspond to 0.38 eV and 0.33 eV excitation temperatures in the 130 A/cm^2 and 13 A/cm^2 cases.

obtained from the measured current density and calculated mobilities,[3,9] from the initial Na density $[Na]_0$. Some of the electrons may result from Xe ionization, but as $n_e/[Na]_0 < 0.35$, this is not a major uncertainty. The resulting residual Na densities as well as $[Na]_0$ are plotted in Fig. 4. It is noteworthy that for each j the measured populations fall nearly on a straight line corresponding to a single excitation temperature.

By varying the electrode gap the voltage drop attributed to the cathode fall has been determined to be ~15 V, out of a typical total voltage drop of 50-100 V. Thus the electric field E in the positive column is known from the electrode voltages. In Fig. 5 E/N and [Na(3P)]/[Na(3S)] are plotted as a function of j/N for the range of conditions covered in the experiment (N = [Xe]). Since the discharge area increases with cell current (I), j does not cover as large a range as I. An extremely valuable result displayed by Fig. 5 is the positive-resistance characteristic of the discharge, a condition that seems to be closely connected to the absence of discharge instabilities and the spreading of the discharge with increasing I.

D. Conclusions.

The ratio $[Na^*(3P)]/[Na(3S)]_0 \sim 0.01$ achieved in the discharge (see Fig. 6) is insufficient for net optical gain on the A-X band at $\lambda \sim 700$ nm, where the gain coefficient is relatively large (i.e., $[Na^*][Na]^{-1}(g/g^*)\exp\{-h(\nu-\nu_0)/kT\}$ must exceed 1).[1,2] There is net gain on this band in the 800-900 nm region, but the gain coefficient is quite small.[10] When Na(3S) depletion is allowed for, as in the lines in Fig. 5, it appears that [Na*(3P)]/[Na(3S)] might reach the desired 0.03 to 0.05 values at $jN_0/N > 10^3$ A cm^{-2}, but the gain coefficient would be small due to neutral Na depletion, and efficiency would be very low.

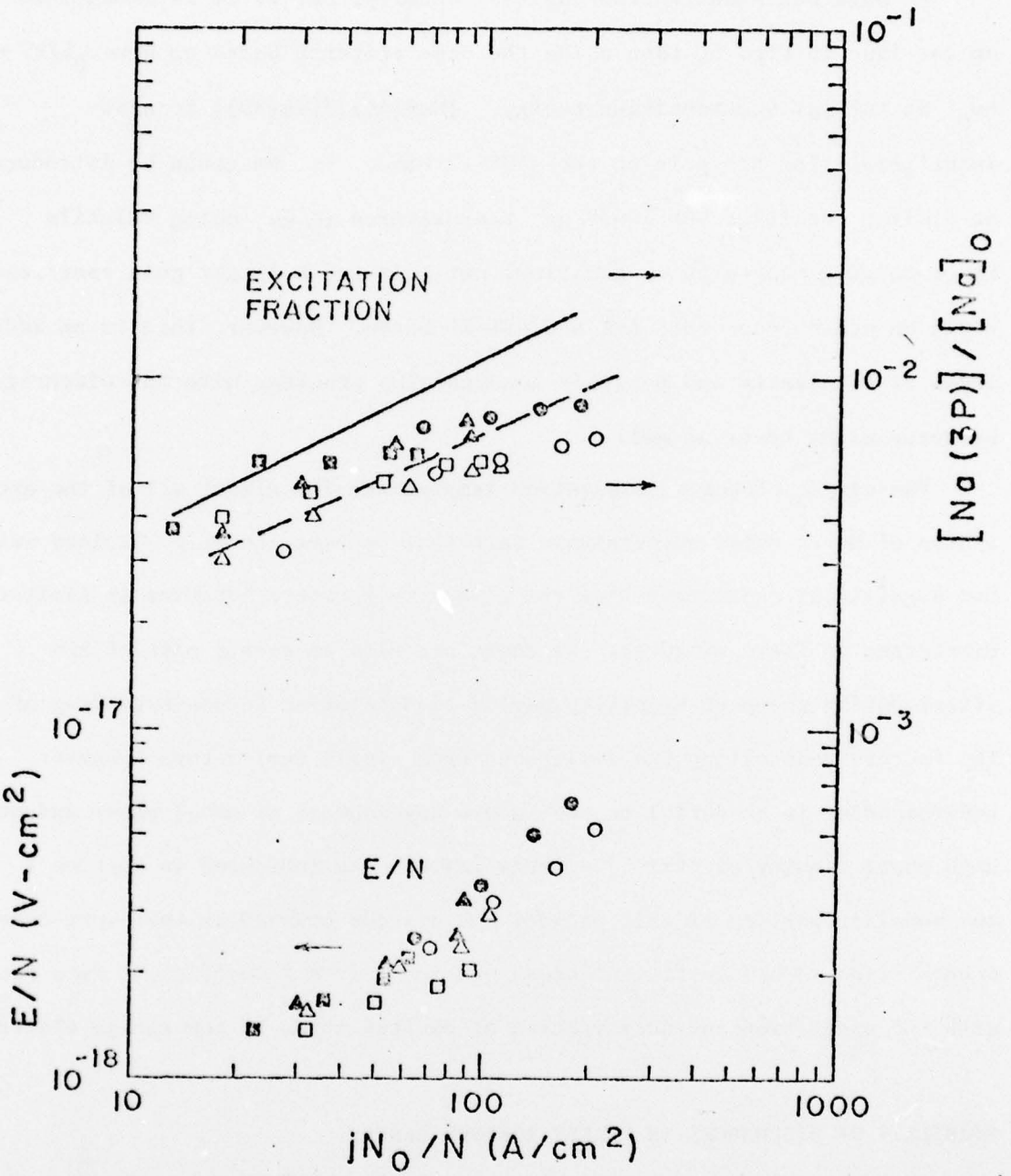

Fig. 5. E/N and $[Na(3P)]/[Na]_0$ in the positive column versus $j(N_0/N)$, where N= [Xe], $N_0 = 2.7 \times 10^{19}$ cm^{-3} and N/N_0 = 2.04 (□ and ■), 1.07 (Δ and ▲), 0.50 (o and •). The ratio [Xe]/[Na] = 3600 for the open symbols and dashed line and 8000 for the solid symbols and solid line. The lines are averages of [Na(3P)]/[Na(3S)] for the same data, where $[Na(3S)] = [Na]_0 - n_e$.

We have not measured the Na*(4S) density, but if it is assumed to fit on the line in Fig. 5, then using the same criteria based on $h(\nu-\nu_0)/kT$ where $h\nu_0$ is the 3s - 4s transition energy, [Na*(4S)]/[Na(3S)] is also insufficient for net gain on the $4S\Sigma$-$X\Sigma$ band. If Na could be introduced at similar densities but lower gas temperatures (e.g., using volatile Na-containing molecules or gas flow) net gain and a larger gain coefficient could be achieved on the A-X and $4S\Sigma$-$X\Sigma$ bands. However, this is an added level of complexity and possible accompanying problems with the discharge behavior might occur as well.

The single effective excitation temperature for almost all of the excited states of Na is quite surprising. Note that we have recently obtained evidence for significant departures from the single temperature behavior in similar discharges in Tℓ-Xe mixtures. We therefore plan to devote most of the effort during the next reporting period to developing an understanding of the factors controlling the deviations from single temperature behavior. This understanding is essential to the future development of metal vapor and other high power density electric discharge lasers. As indicated in Section I the modeling portion of this project has already started on this work through the accumulation and evaluation of cross section and rate coefficient data concerned with the excitation and deexcitation of excited atoms by low energy electrons.

III. STABILITY OF DISCHARGES IN WEAKLY IONIZED GASES.

Drs. H. C. Chen (to 4/77), W. L. Morgan (from 6/76) and A. V. Phelps.

In the last semiannual report we presented a summary of the techniques we have developed for the modeling of the growth of the cathode fall region of a glow discharge such as found in high pressure lasers. During the portion of this reporting period before the end of Dr. Chen's appointment, the results

of our cathode fall model were compared with the available experimental data. The principle results of this comparison are shown in Figures 6 and 7. In Figure 6 we show the "raw data" of the experiment and theory for cathode falls in helium. This plot takes advantage of the scaling laws formulated earlier so as to plot all of the available data in a form which should yield unique curves of cathode fall voltage and sheath thickness times pressure vs. current density divided by pressure squared. The scale at the top of Figure 6 is appropriate to discharges in helium at a pressure of 1000 torr. We see that the open points representing relatively low pressure experiments and the solid points representing high pressure theory do scale as expected. The solid lines are the results of a very simple steady-state model in which the secondary emission coefficient and electron and ion mobilities are assumed constant and only the positive ion space charge is taken into account.

The data of Figure 6 has been replotted in Figure 7 so as to show the power dissipation and electric field strength to gas density ratio to be expected in the cathode fall region. For example, this scaling indicates that for a current density of 100 A/cm^2 at 1000 torr the cathode fall voltage is 400 volts, the sheath thickness is 10 μm, the power input to the sheath is 40 kW/cm^2 or 40 MW/cm^3, and the average electric field strength is 10^5 V/cm. It should be kept in mind that this scaling neglects gas and electrode heating as in a very short pulsed discharge, e.g., 10 ns. Also, essentially no quantitative experimental data is available or likely to become available for quantities such as sheath thickness at these high pressures.

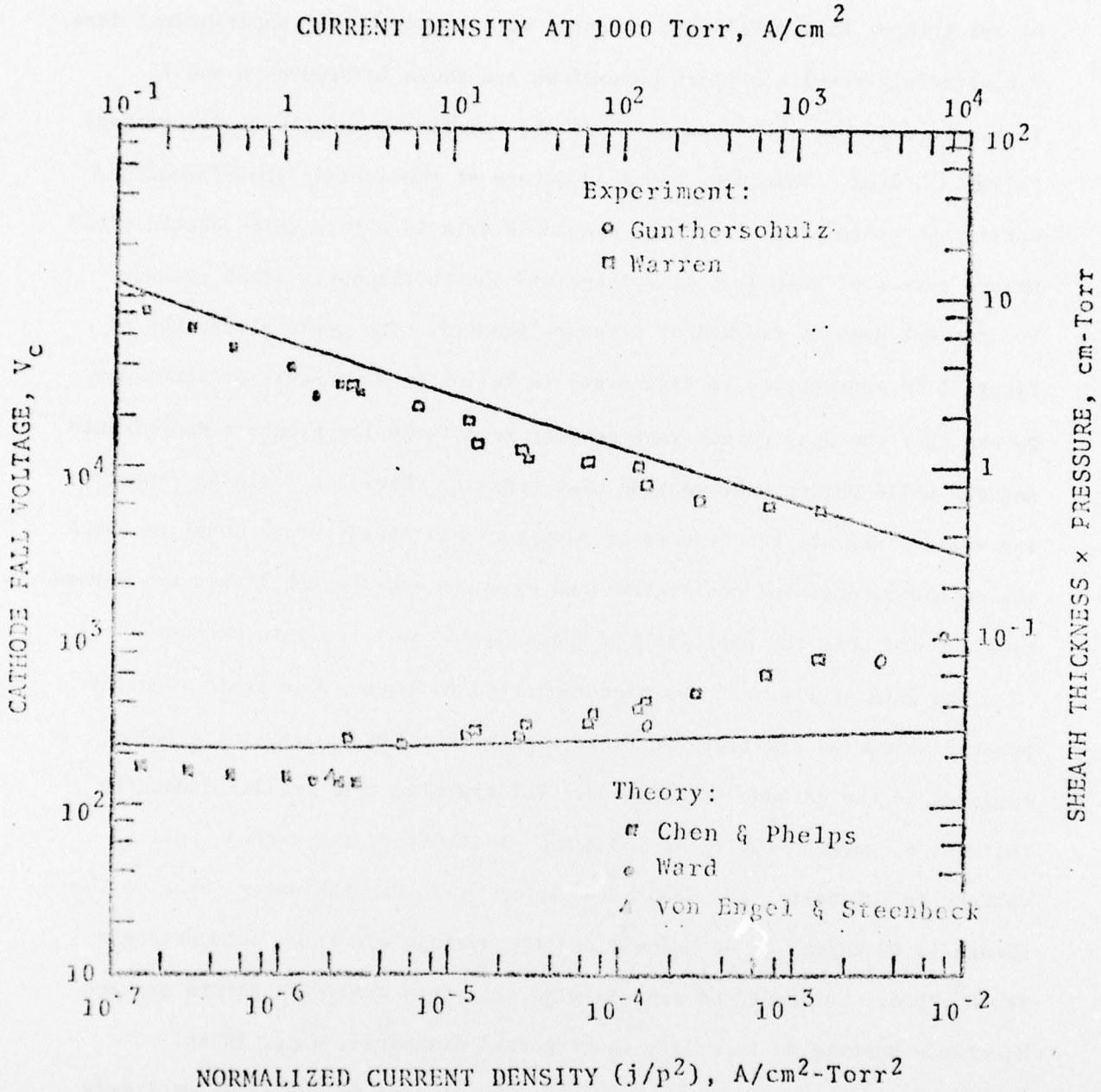

Fig. 6. Cathode fall characteristics for discharges in helium. The upper scale shows current densities for a discharge in helium at 1000 torr. See text for other conditions.

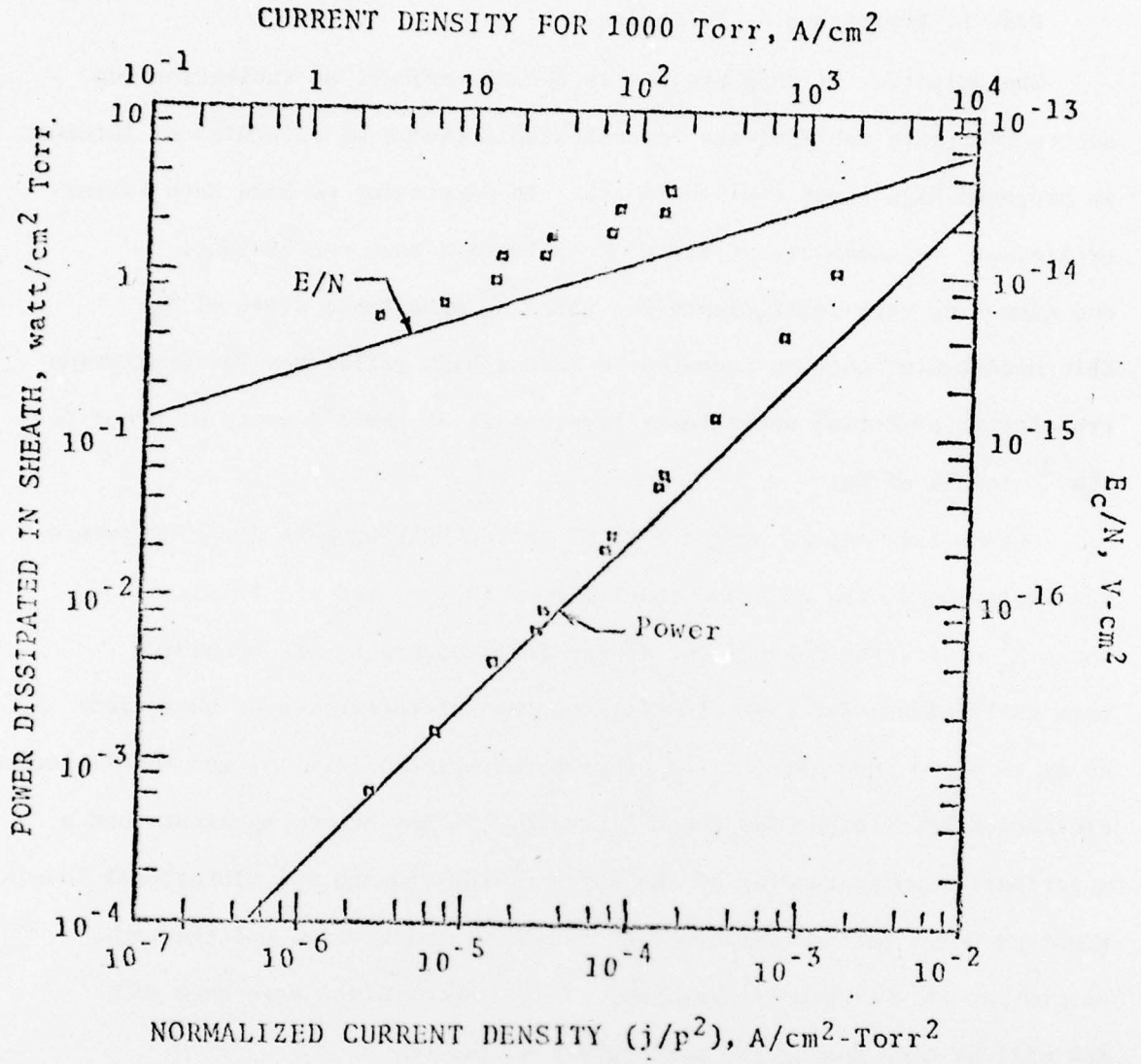

Fig. 7. Power input and mean E/N value for cathode fall region of discharges in helium.

IV. ELECTRON EXCITATION OF MOLECULAR METASTABLES

Drs. D. Levron and A. V. Phelps.

The objective of this project is the measurement of excitation and destruction rate coefficients for metastable states of molecules of interest in proposed high power visible lasers. In particular we have been making preliminary measurements of electron excitation rate coefficients and quenching rate coefficients for the $A^3\Sigma_u^+$ metastable state of N_2. This metastable state is reported to have a high efficiency for excitation transfer to potential upper laser levels such as the $A^3\Sigma$ state of NO or to the ^3P levels of Hg.

During this report period most of the effort has been directed toward the isolation of the emission spectra from the v=0 and v=1 levels of the $A^3\Sigma_u^+$ state, the measurement of the decay constants and quenching rate coefficients for these levels, and the interpretation of these data so as to yield the contribution of each vibrational level to the total electron excitation coefficient for the $A^3\Sigma_u^+$ state. It has become apparent that a quantitative understanding of the roles of the v=0 and v=1 vibrational levels required still further improvements in the uv calibration and the time resolution of the detection system. These improvements have been made and will be used during the next reporting period.

V. SCATTERING AND TRANSPORT OF RESONANCE RADIATION.

Drs. A. Zajonc and A. V. Phelps.

The immediate objective of this project is the testing of theories of radiative and nonradiative transport of resonance excitation in sodium vapor at wavelengths near the peak of the resonance lines. As indicated in

Section I, the present emphasis on the effects of nonradiative transport of resonance excitation arises from its potential importance in understanding and predicting the decrease in the efficiency of laser pumping experiments when pumping occurs at line center.

Recent work has been concerned with the improvement in the procedures for the transfer of sodium into the experimental cell, the improvement of the normalization of measured fluorescent intensities to account for changes in laser intensity and beam position and focusing, the preliminary measurement of fluorescent intensities and line profiles, and the modification of the computer code[11] which predicts the measured spectral intensities.

Figure 8 shows the predicted variation in the fluorescent intensity as the incident laser is tuned through the resonance. In this case the laser is tuned through the D_1 line of Na (589.0 nm) and the monochromator and detector are adjusted to observe the fluorescence of the D_2 line (589.6 nm). The solid curves are calculated assuming no reflection of excited atoms striking the window of the cell. The curve labled D assumes that the diffusion coefficient for the excited atoms is the value calculated[12] using the conventional formulas for the frequency of excitation transfer collisions to determine the mean-free-path. The other two solid curves show the expected fluorescence when the diffusion coefficient for the excited atoms is increased or decreased a factor of 10. The dashed curve shows the profile expected when the reflection coefficient for the excited atoms at the window is increased to 100%. We see that at a sodium density of 10^{15} cm^{-3} the predicted reduction in fluorescence and pumping efficiency at line center due to nonradiative transport is about a factor of five. During the next reporting period we expect to modify the theory to include hyperfine structure, to complete the fluorescence measurements and to compare theory and experiment.

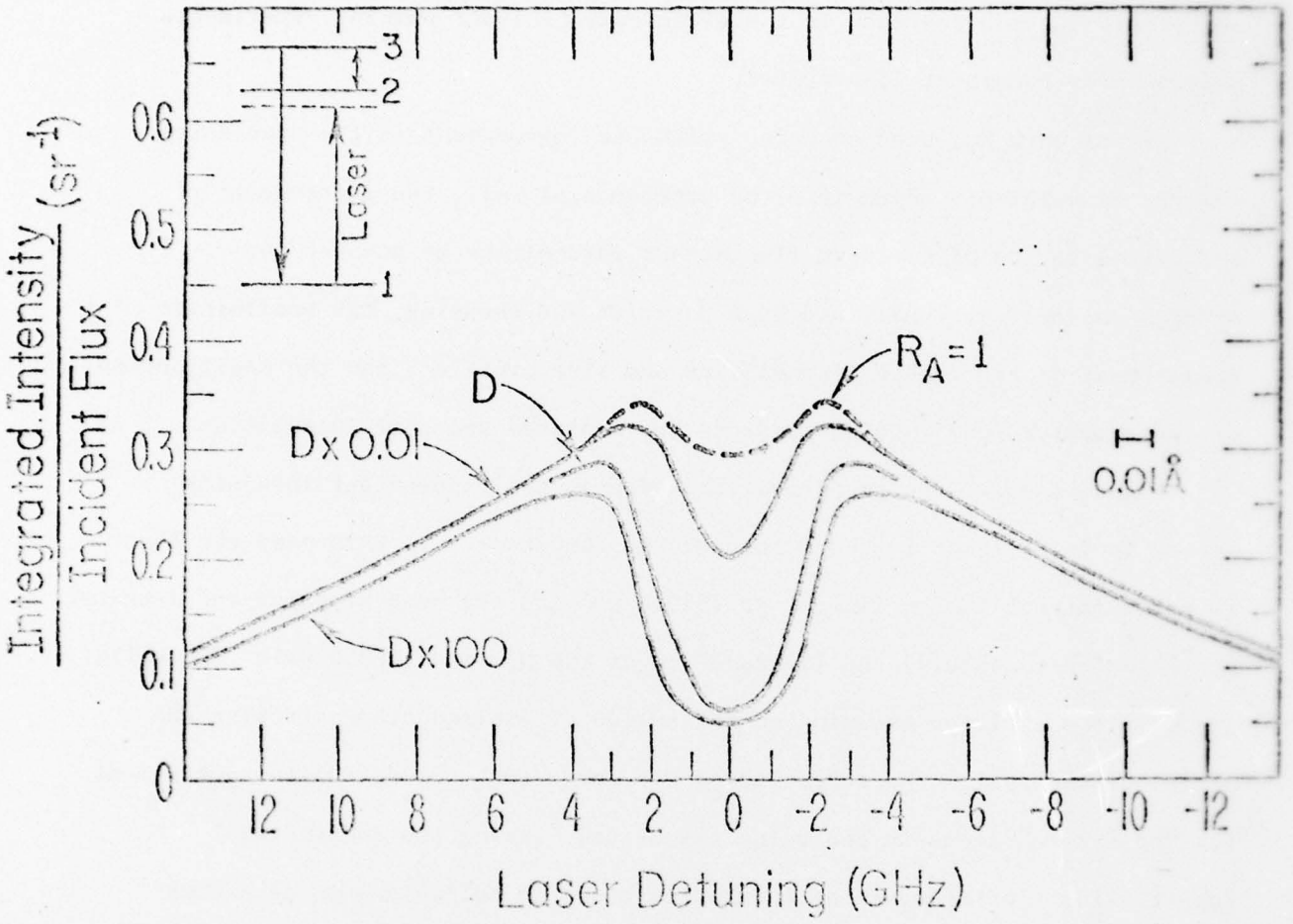

Fig. 8. Theoretical fluorescent intensity vs. laser frequency relative to line center for Na vapor at 10^{15} atom/cm^3. The solid curves show the effect of variations in the assumed excited atom diffusion coefficient. The dashed curve shows the effect of assuming complete reflection of the excited atoms at the window.

REFERENCES

1. A. V. Phelps, "Tunable Gas Lasers Utilizing Ground State Dissociation," JILA Report 110 (Joint Institute for Laboratory Astrophysics, University of Colorado, Boulder, CO, 1972).
2. G. York and A. Gallagher, "High Power Gas Lasers Based on Alakli-Dimer A-X Band Radiation," JILA Report 114 (Joint Institute for Laboratory Astrophysics, University of Colorado, Boulder, CO, 1974).
3. R. Shuker, L. Morgan, A. Gallagher and A. V. Phelps, in preparation and Bull. Am. Phys. Soc. 23, 142 (1977).
4. D. Leep, Ph.D. thesis, University of Colorado, 1977 (unpublished).
5. G. York, R. Scheps and A. Gallagher, J. Chem. Phys. 63, 1052 (1975).
6. A. Tam, G. Moe, B. Bulos and W. Happer, Opt. Comm. 16, 376 (1976).
7. L. Lam, A. Gallagher and M. Hessel, J. Chem. Phys. 66, 3550 (1976).
8. W. L. Wiese, M. W. Smith and B. M. Miles, Atomic Transition Probabilities, NSRDS-NBS 22 (USGPO, Washington, DC, 1969).
9. L. A. Schlie, Bull. Am. Phys. Soc. 21, 172 (1976); J. Appl. Phys. 47, 1397 (1976).
10. R. P. West, P. Shuker and A. Gallagher, J. Chem. Phys., in press (1978).
11. D. G. Hummer and P. B. Kunasz, J. Quant. Spectrosc. and Rad. Transfer 16, 17 (1976); C. Kunasz and P. B. Kunasz, Compt. Phys. Comm. 10, 304 (1975).
12. A. V. Phelps and A. O. McCoubrey, Phys. Rev. 118, 1561 (1960).